LAWRENCE
LIVERMORE
NATIONAL
LABORATORY

UCRL-TR-218181

Neutron Induced Cross Sections for Radiochemistry for Isotopes of Arsenic

K. Kelley, R. D. Hoffman, F. S. Dietrich, M. Mustafa

January 17, 2006

This work was performed under the auspices of the U.S. Department of Energy by University of California, Lawrence Livermore National Laboratory under Contract W-7405-Eng-48.

UCRL-TR-218181

Neutron Induced Cross Sections for Radiochemistry for Isotopes of Arsenic

K. Kelley, R. D. Hoffman, and F. S. Dietrich
Nuclear Theory and Modeling Group
Physics and Advanced Technologies, N-Division
Lawrence Livermore National Laboratory
Livermore, CA 94550
kelley24@llnl.gov

M. Mustafa
Nuclear and Defense Technologies, AX-Division
Lawrence Livermore National Laboratory
Livermore, CA 94550

January 17, 2006

ABSTRACT

We have developed a set of modeled nuclear reaction cross sections for use in radiochemical diagnostics. Local systematics for the input parameters required by the Hauser-Feshbach statistical model were developed and used to calculate neutron induced nuclear reaction cross sections for isotopes of Arsenic ($Z = 33$) in the mass range $71 \leq A \leq 77$.

Subject headings: Nuclear cross sections, Radiochemistry, Nuclear Physics

1. Introduction

1.1. Radiochemistry

Various aspects of nuclear explosive device performance can be determined through the use of radiochemistry. During the UGT (Under Ground Test) Program, select naturally occurring elements were included prior to a test and their activation products subsequently retrieved for counting, typically with gamma-ray detectors. The products were measured as isotopic ratios (such as ^{87}Y/^{88}Y produced from the stable isotope of the naturally occurring element). From the measured activity and prior knowledge of the amount of loaded detector material, performance aspects could be inferred by comparing the measured isotope ratios with those calculated using neutron and charged-particle fluences from one of the design codes and group-averaged cross section sets prepared for this purpose.

This paper develops the first Arsenic cross section set for the LLNL RADCHEM library (Nethaway 1998). In previous efforts we have performed similar analysis for several other neutron or charged particle detector sets, including ^{79}Br producing ^{79}Kr (Hoffman *et al.* 2004a), ^{127}I producing ^{127}Xe (Hoffman *et al.* 2004b), stable europium producing $^{147-150,152,154}$Eu and ^{151,153}Gd (Hoffman *et al.* 2004c), natural titanium producing ^{48}V or $^{46-48}$Sc, stable ^{52}Cr producing ^{52g}Mn, and stable ^{54}Fe producing ^{52g}Mn (Kelley *et al.* 2005). This paper details the unclassified cross section modeling effort. A separate classified document will discuss Stockpile Stewardship applications.

Contents

List of Figures

List of Tables

1.2. Other Available Cross Section Sets

This effort develops the first As detector set cross sections for the LLNL RADCHEM library. A recent evaluation of the important cross sections related to the production of ^{73,74}As is provided by (Pruet 2005).

1.3. Proposed As Detector Set

We consider as targets isotopes of arsenic with mass numbers $71 \leq A \leq 77$. This includes any long-lived isomers with half-lives greater than 1 μs. We have calculated nuclear reaction cross sections for incident neutrons on these targets with laboratory incident neutron energies ranging from 0.01 keV to 20 MeV. These compound systems are then allowed to decay through the (n,γ), (n,n'), (n,2n), (n,3n), (n,p), (n,np), (n,pn), (n,α), and (n,d) reaction channels.

Our goal is to develop a consistent set that reproduces, as closely as possible, measured cross sections on targets in the *local region of interest*. To do this we develop *local systematics* for the many input quantities used in the theoretical reaction modeling calculations. These systematics are based on experimental data that are often only available for compound nuclear systems formed from a stable target plus a neutron. Of course, we use experimental data whenever it is available, but reactions proceeding through unstable systems are unavoidable in radiochemistry. Short of developing new experimental techniques to measure cross sections on unstable targets, our only hope is to develop cross section sets that reproduce well the measured cross sections in the region of interest.

In §2 we describe the theoretical techniques used in the modeling effort. §3 describes the input parameters. §4 gives results. We conclude with §5.

2. Nuclear Reaction Theory

2.1. Reaction Mechanisms

Conceptually, we consider nuclear reaction mechanisms to be of two general types, direct processes and compound processes. Direct processes can be pictured as simple interactions of the incident particle with the nuclear potential of the target nucleus. They proceed on a rapid time scale (of order $\sim 10^{-22}$ s), and the reaction products are often highly peaked in the incident particle direction. Compound processes are pictured as complicated interactions proceeding over a much longer timescale ($10^{-15} - 10^{-18}$ s) in which the reaction is mediated by the formation of a "compound nucleus", with the excitation energy of the incident particle being statistically "shared" with the ensemble of nucleons in the target over all energetically allowed degrees of freedom. The reaction products are largely isotropic. Compound nuclear reactions proceed through resonances, which correspond to nuclear states above the bound region, while direct reactions proceed through smooth potential terms. Other intermediate reaction mechanisms may exist between these two extremes. We refer to these as "pre-compound" nuclear processes.

Over the energy range of interest to this project, a few keV to 20 MeV, we consider pre-compound and compound nuclear processes, with the pre-compound reactions operating principally above 10 MeV of incident particle excitation energy.

2.2. Hauser-Feshbach Statistical Model

A traditional theoretical approach to compound nuclear reactions is the statistical or Hauser-Feshbach model (Hauser & Feshbach 1952). This model is valid only for high level densities in the compound nucleus, allowing one to use energy averaged transmission coefficients T, which describe absorption via an imaginary part in the (optical) nucleon-nucleus potential. For the reaction I (in state μ) $+j \rightarrow k +$ L (in state ν), with $\mathrm{I}^{\mu} + j$ interacting with center-of-mass energy E_j^{μ} (in MeV), the average cross section is given by

$$\sigma_{jk}^{\mu\nu}(E_j^{\mu}) = \frac{\pi \lambda\!\!\!^{-2}_j}{g_I^{\mu} g_j} \sum_{J,\pi} g_J \frac{T_j^{\mu}(J^{\pi}) T_k^{\nu}(J^{\pi})}{T_{tot}(J^{\pi})} W(J^{\pi}) \tag{1}$$

where the summation extends over all compound nuclear spins and parities J^{π}, μ and ν are states in the target and product (=0 for the ground state, 1 for the 1^{st} excited state, etc.). The cross section has units of area, described by $\pi \lambda\!\!\!^{-2}_j = 0.6566(\hat{A}_j E_j^{\mu})^{-1}$ barns, with $\hat{A}_j = (A_I A_j)/(A_I + A_j)$ being the reduced mass in atomic mass units and E_j^{μ} is the center of mass energy in units of MeV. $\lambda\!\!\!^{-}_j$ is the wavelength related to the wave number k_j in the target plus incident particle channel by $\lambda\!\!\!^{-}_j = 1/k_j$ The statistical weights are given by $g_y^x = (2J_y^x + 1)$. Items without superscripts refer to the compound nucleus.

The transmission coefficients in the numerator are the total transmission coefficient for forming the state J^{π} in the compound nucleus $I^{\mu} + j$ at energy E_j^{μ}, given by $T_j^{\mu}(J^{\pi})$. $T_k^{\nu}(J^{\pi})$ is the same

as $T_j^\mu(J^\pi)$ but for the pair $L^\nu + k$ at energy E_k^ν. Implicit in these definitions is a sum over all possible $l-$waves and channel spins, i.e.

$$T_j^\mu(J^\pi) = \sum_{l,s} T_j^\mu(J^\pi, l, s) \qquad (2)$$

where l is any partial wave number (orbital angular momentum) that can couple the state μ to the compound nuclear state having spin and parity J^π subject to quantum mechanical selection rules and s is the vector sum of the spins J_I^μ and J_j. Hence s takes on all integer (or half-integer) numbers from $|J_I^\mu - J_j|$ to $J_I^\mu + J_j$.

T_{tot} represents the sum of transmission coefficients over all possible decay channels (i.e. for all particles and photons). The cross section for the formation of species L, regardless of its state ν, is obtained by summing Eq. [1] over all bound states ν of L for which the reaction is energetically allowed.

When evaluating these sums, if energies become of interest which exceed the highest discrete excited state for which energy, spin, and parity are explicitly known, a nuclear level density formula must be employed. Specifically, the definitions for the transmission coefficients $T_j(J^\pi)$, $T_k(J^\pi)$, and $T_{tot}(J^\pi)$ must be modified, for example:

$$T_k(J^\pi) = \sum_{\nu=0}^{\omega} T_k^\nu(J^\pi) + \int_{\xi_L^\omega}^{\xi_L^{max}} \int_{J^\nu \pi^\nu} T_k^\nu(\xi_L^\nu, J^\pi)\rho(\xi_L^\nu, J^\nu, \pi^\nu) d\xi_L^\nu d\pi^\nu dJ^\nu$$

where for the nucleus L, ξ_L^ω is the energy of the highest excited state, ω, of known energy, spin, and parity; $\xi_L^{max} = E_k^0 = E_j^0 + Q_{jk}$ is the maximum excitation energy available, and $\rho(\xi_L^\nu, J^\nu, \pi^\nu)$ is the density of states per unit energy of spin and parity J^ν and π^ν at the excitation energy ξ_L^ν. The above integral approximates a summation and is subject to the same quantum mechanical restrictions implied in the definition of the transmission function.

2.3. Width Fluctuations

In addition to the transmission coefficients for particles and photons and level densities required for Eq. [1], width fluctuation corrections (WFC, $W(J^\pi)$ in Eq. [1]) must also be employed. They define the correlation factors with which all partial channels of incoming particle j and outgoing particle k, passing through excited state (E, J, π), have to be multiplied. The major effect is to enhance the elastic channel and accordingly decrease the other open channels. These effects are most often observed at or near channel opening energies when i.e. a (p,γ) and a (p,n) channel compete and the weaker (p,γ) channel is enhanced. Above a few MeV of excitation energy, when many competing channels are open, WFC's can be neglected.

The exact expression for the WFC, obtained with the Gaussian orthogonal ensemble (GOE) approach, requires the evaluation of a triple integral and to date has been considered much to costly to apply in nuclear cross section calculations. Several approximations have been developed, the most popular ones are the Moldauer model (Moldauer 1976), and the HRTW model (Hofmann *et al.* 1975). We use the Moldauer model approximation in this study. For a detailed description of the full (GOE) treatment and a comparison with the Moldauer and HRTW approximation models mentioned above, see (Hilaire Lagrange & Koning 2003).

2.4. Pre-Compound Processes

For excitation energies starting around 10 MeV, pre-compound processes become important. We account for the pre-equilibrium emission of particles from the first compound nucleus using a simple exciton model. In the pre-equilibrium stage of the reaction, particle emission is assumed to be the only decay mode. Once the pre-equilibrium cross section leading to the appropriate final state has been calculated, the total pre-equilibrium cross section is subtracted from the reaction cross section. The reaction then proceeds through the usual statistical channels (Eq. [1]). Pre-compound processes are generally important only for the first compound nucleus. Subsequent (higher chance) processes are treated as sequential evaporation steps. After the Hauser-Feshbach portion of the calculation is complete, the pre-equilibrium cross section leading to the desired final state is added back to the statistical model cross section.

2.5. The STAPRE Hauser-Feshbach Reaction Code

We adopt the statistical model code STAPRE (STAatistical-PREequilibrium) to model our cross sections (Uhl & Strohmaier 1976). It embodies all of the physical models discussed above. The version of the code we use is STAPRE-H95 (Avrigeanu & Avrigeanu 1976), available from the NEA web site. We have made several modifica-

tions, primarily to the level density routines. Prior versions of the code were used to develop parts of the existing RADCHEM data sets (Vonach 1982).

In the following we discuss the important ingredients of statistical model calculations, and the methods used to estimate them. These are the requisite nuclear structure data (energies, spins, and parities of the ground states and all known excited states, as well as detailed branching ratios for the gamma-ray cascade from excited to low-lying states), the width fluctuation corrections, the pre-compound cross section, the particle and γ-transmission coefficients, and the nuclear level densities of all nuclei involved in the reaction. The reliability of such calculations is chiefly determined by the accuracy with which these components can be evaluated.

3. Inputs Required for the Hauser-Feshbach Model

3.1. Nuclear Structure Data

3.1.1. Nuclear Masses and J^π Assignments

We adopt the experimental mass excess values of (Wapstra Audi & Thibault 2003), as listed in Appendix 3. Spin and parity assignments are from the Evaluated Nuclear Structure Data File (ENSDF 2003). We present in Table 3 (Appendix A.1) the binding energies (in MeV) calculated from the adopted masses, the ground state spins and parities, and the separation energies for neutrons, protons, alpha-particles, and deuterons for the nuclei included in this study. In Table 4 (Appendix A.2), we provide reaction Q-values for the cross sections calculated in this study.

3.1.2. Nuclear Level Schemes

The nuclear structure data needed to model the gamma-ray cascade in this study was adopted from the file BUDAPEST.DAT (RIPL 1998). The number of excited levels adopted for each nucleus is given as the quantity "N" in Table 5 (Appendix A.3). For the unmodified isotopes, this was the number for which energy spin and parity were unambiguously assigned in the BUDAPEST file. Nuclei for which only a ground state was used are indicated by N=0. The discrete level schemes for $^{72-76}$As are shown in Figure 11 (Appendix A.4).

3.2. Transmission Coefficients

3.2.1. Neutron and Proton Optical Potentials

For the calculation of the neutron and proton particle transmission coefficients, we use the optical model of (Koning & Delaroche 2001). Although they have tuned their parameters to fit data for many different species (see their Tables 6 and 7), we decided to use the global nucleon-nucleon optical model potential (OMP), as it gives a very satisfactory fit to measured total cross section data for neutrons and protons in the range of interest to us. Specifically, we adopt the potential depth parameters and Fermi energies for the neutron and proton global OMP defined in their Section 5.2, tables 14 and 15. The particle transmission coefficients were generated by the optical model code ECIS-95 (Raynal 1996). Although designed for coupled channel calculations, we used the code in a spherical optical model mode.

We present in Figure (1) results of the Koning & Delaroche optical model compared to measured total neutron cross sections for select targets in our region of interest. In each instance, the optical model closely replicates the experimental data. The optical model result predicts average cross sections, not the resonance structure that is generally present at lower energies (e.g. the low energy data for ^{75}As). For additional comparisons, see (Koning & Delaroche 2001). This optical model has produced similar favorable comparisons to measured total neutron cross sections in the regions of scandium, titanium, vanadium, chromium, manganese, and iron (Kelley *et al.* 2005), bromine and krypton (Hoffman *et al.* 2004a), and iodine and xenon (Hoffman *et al.* 2004b). There is some evidence that the proton transmission coefficients derived from this optical potential may be too large for lighter nuclei (Kelley *et al.* 2005). Such a large proton transmission coefficient will primarily affect modeled (p,n) and (n,p) cross sections but should have little impact on the (n,γ) and (n,2n) cross sections that dominate the production of radioactive ^{73,74}As from loaded ^{75}As.

3.2.2. The Alpha and Deuteron Optical Potentials

We have included possible alpha and deuteron exit channels in this modeling effort. For the alpha particles, we use the optical potential of (McFadden & Satchler 1966), and for deuterons we use that of (Perey & Perey 1963), as encoded in the SCAT2 subroutine of STAPRE-H95.

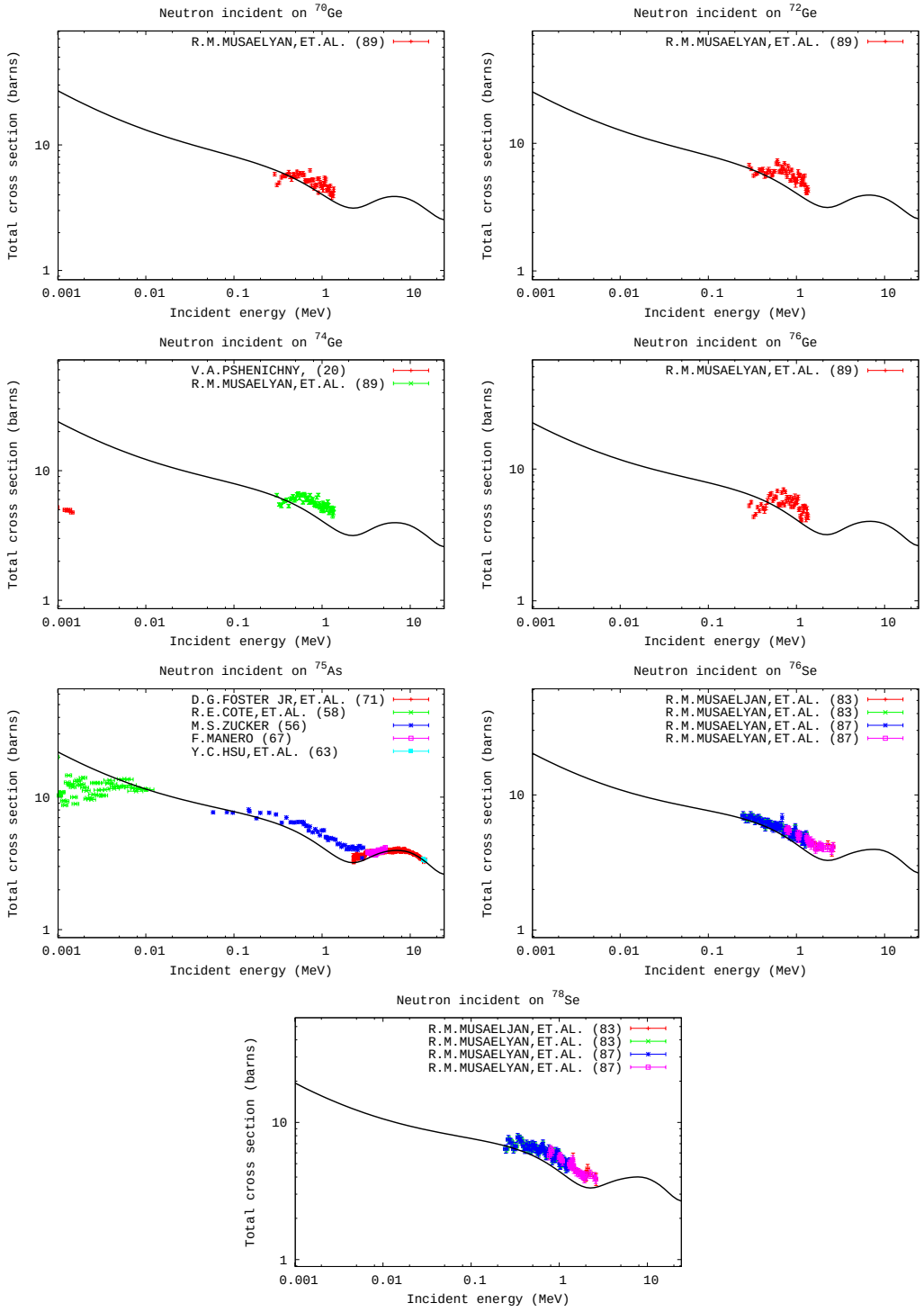

Fig. 1.— Total measured neutron cross sections vs those predicted by the optical model of Koning-Delaroche for select targets in the range $32 \leq Z \leq 34$, $38 \leq N \leq 44$. Measured values were obtained from (CSISRS 2003). The optical model prediction is indicated by the solid black line.

We do not include a quality analysis of these potentials in this report. The deuteron and alpha exit channels are small when compared to the dominant channel, accounting for less than 10% of the total reaction cross section in all cases, less than 5% in most. Therefore, any sensitivity to

the alpha and deuteron potentials will only be apparent in these weak exit channels. Additionally, somewhat reasonable agreement with the experimental ^{75}As(n,α) cross section provides us with a degree of confidence in the alpha potential (see Figure 5).

3.2.3. Transmission Coefficients for Photons

For the calculation of the gamma ray transmission coefficients, we use a simple model where the transmission coefficient depends only on the multipole type (XL) and the transition energy (ϵ), as encoded in STAPRE (Avrigeanu & Avrigeanu 1976). They are related to the gamma ray strength function $f^{\gamma}_{XL}(\epsilon)$ by

$$T^{\gamma}_{XL}(\epsilon) = 2\pi\epsilon^{2L+1} f^{\gamma}_{XL}(\epsilon) \quad (3)$$

The energy dependence of the strength function was determined using the GDR model with simple Lorentzian line shapes. In particular, the E1 strength function is given by

$$f^{\gamma}_{E1}(\epsilon) = \mathcal{N}\zeta\sigma_G \frac{\Gamma_G^2\epsilon}{\left(\epsilon^2 - E_G^2\right)^2 + \left(\Gamma_G\epsilon\right)^2} \ (\mathrm{MeV}^{-3}) \quad (4)$$

where E_G, Γ_G, and σ_G are the energy, width, and peak cross section of the Giant Dipole Resonance given in MeV and mb respectively. The constant ζ is 8.674×10^{-8} mb^{-1}·MeV^{-2}. The GDR parameters are given by

$$\begin{aligned} E_G &= \frac{80 \text{ MeV}}{A_C^{1/3}} \\ \Gamma_G &= 5 \text{ MeV} \\ \sigma_G &= A_C \frac{13 \text{ mb}}{5} \end{aligned} \quad (5)$$

where A_C is the mass number of the compound nucleus. We also include M1, E2, and M2 transitions. Their transmission coefficients are simply proportional to ϵ^{2L+1}, and therefore their strength functions are constants. In particular,

$$\begin{aligned} f^{\gamma}_{M1}(\epsilon) &= 3.1\times10^{-1} A_C^{-2/3} f^{\gamma}_{E1}(S_n) \\ f^{\gamma}_{E2}(\epsilon) &= 7.2\times10^{-7} A_C^{2/3} f^{\gamma}_{E1}(S_n) \\ f^{\gamma}_{M2}(\epsilon) &= 2.2\times10^{-7} f^{\gamma}_{E1}(S_n) \end{aligned} \quad (6)$$

where S_n is the neutron separation energy. In all cases, E1 is the dominant multi-pole radiation.

The factor $\mathcal{N}$ appearing in Eq. 4 is a normalization constant, determined by fitting the average total s-wave radiation width at the neutron binding energy,

$$\langle\Gamma_\gamma\rangle_0 = \frac{J+1}{2J+1}\left\langle\Gamma_\gamma\left(B_n, J+\frac{1}{2}\right)\right\rangle + \frac{J}{2J+1}\left\langle\Gamma_\gamma\left(B_n, J-\frac{1}{2}\right)\right\rangle \quad (7)$$

$$\Gamma_\gamma(E,J) = \frac{T_\gamma(E,J)}{2\pi\rho(E,J)} \ (\mathrm{meV})$$

(Uhl & Strohmaier 1976). Here, J is the spin of the target nucleus. The gamma-ray transmission coefficient is evaluated as in Eq. 3. Since the total s-wave radiation width is generally measured only for stable isotopes plus a neutron, we have developed a systematic approach for estimating this value for the many unstable nuclei in our region of interest. The systematic values are determined by a least squares quadratic fit to experimental data (Figure 2). Using measured radiation widths for compound nuclei in the range $28 \le Z \le 35$, $36 \le N \le 44$, we find the systematic

$$\langle\Gamma_\gamma\rangle_0^{\text{sys.}} = 3.2359\times A^2 - 474.71\times A + 17630. \quad (8)$$

We use the experimental values for all systems that have measured average s-wave radiation widths. The systematic is used for all others.

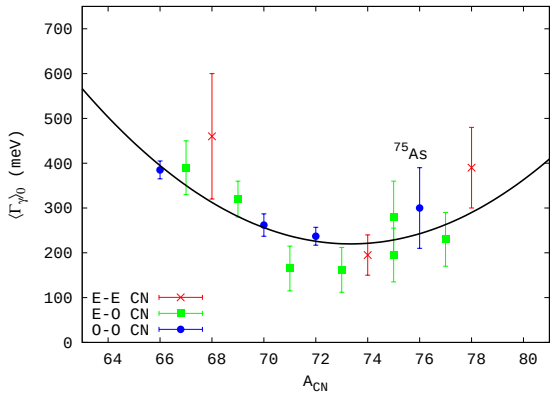

Fig. 2.— Systematic for the average total s-wave radiation width. Measured values are from (RIPL 1998). Data for even-Z even-N, even-Z odd-N, and odd-Z odd-N compound nuclei are shown in red, green, and blue, respectively. No odd-Z even-N data exists in this local region of interest. The solid black line represents our systematic, described in the text.

3.3. Nuclear Level Densities

Another important input to the statistical model code is the nuclear level density. For this project, we have adopted a standardized, semi-empirical approach which is numerically efficient, can be tied to experimental data, and is fairly

accurate. The level density is described by two functions. Both are energy dependent, the second factor contains the spin dependence. This is the "Back-shifted Fermi Gas" formulation of the nuclear level density:

$$\rho\left(U,J\right)=\rho\left(U\right)f\left(U,J\right) \tag{9}$$

where $\rho(U)$ is the state density, with $U=E-\Delta$ the back-shifted energy. Δ is the so called "back-shift", and J is the spin of the compound nucleus. We will further treat each component of Eq. 9 in two ways, depending on the excitation energy of interest. The demarcation point will be roughly between the energy range of the known excited levels of a given compound nucleus (the low energy domain), and near (and above) the neutron binding energy (the high energy domain).

The process of developing local systematics for the level density has been thoroughly described in previous papers (Hoffman *et al.* 2004a; Hoffman *et al.* 2004b; Hoffman *et al.* 2004c; Kelley *et al.* 2005), and we will only touch on the more salient points in the present work. For the high energy domain, we describe the level density assuming a backshifted Fermi gas formula,

$$\rho\left(U\right)=\frac{\sqrt{\pi}}{12}\,\frac{\exp\left(2\sqrt{aU}\right)}{a^{1/4}U^{5/4}}\,\frac{1}{\sqrt{2\pi}\sigma} \tag{10}$$

$$f\left(U,J\right)=\frac{2J+1}{2\sigma^{2}}\,\exp\left[\frac{-\left(J+\frac{1}{2}\right)^{2}}{2\sigma^{2}}\right] \tag{11}$$

where $a(U)$ is the level density parameter (in MeV^{-1}) and U is the backshifted energy given by $U=E-\Delta$ with

$$\begin{aligned}\Delta(Z,N) &= \frac{\Delta_p+\Delta_n}{2} \\ \Delta_p\left(Z,N\right) &= E^G\left(Z,N\right) \\ &- \frac{1}{2}E^G\left(Z-1,N\right) \\ &- \frac{1}{2}E^G\left(Z+1,N\right) \\ \Delta_n\left(Z,N\right) &= E^G\left(Z,N\right) \\ &- \frac{1}{2}E^G\left(Z,N-1\right) \\ &- \frac{1}{2}E^G\left(Z,N+1\right)\end{aligned} \tag{12}$$

where $E^G\left(Z,N\right)$ is the binding energy of the nucleus (Z,N). In calculating the binding energies of the various nuclei, we used the experimental mass excesses of (Wapstra Audi & Thibault 2003). The spin cutoff parameter σ^2 is defined as

$$\sigma^{2}=\left(0.1223\right)^{2}A^{5/3}\sqrt{\frac{U}{a}} \tag{13}$$

We adopt the so-called "microscopic correction" from (Möller *et al.* 1995) as our shell corrections, similar to (Rauscher *et al.* 1997), i.e. $\delta W = E_{mic.}$.

Given Δ and σ^2, the level density parameter $a(U)$ can be related to the average "S"-wave level spacing at the neutron binding energy (D_0) where such quantities are measured. In particular we assume an energy dependent level density parameter

$$a(U)=\tilde{a}\left[1+\delta W\frac{f(U)}{U}\right] \tag{14}$$

with $f(U)=1-\exp(-\gamma U)$ (Iljinov *et al.* 1992). We further assume that $\tilde{a}$ is of the form $\tilde{a}=\alpha A+\beta A^{2/3}$, similar to (Rauscher *et al.* 1997). Using the relation

$$D_0^{\mathrm{calc}}=\frac{2}{\rho\left(U,J=\frac{1}{2}\right)} \tag{15}$$

for nuclei with spin $s=0$ and

$$D_0^{\mathrm{calc}}=\frac{2}{\rho\left(U,J=s+\frac{1}{2}\right)+\rho\left(U,J=s-\frac{1}{2}\right)} \tag{16}$$

for nuclei with $s\neq 0$, we numerically solve for the values of α, β, and γ that minimize the quantity

$$\chi^{2}=\sum_{i}\left(\frac{D_0^{\mathrm{calc}}-D_0^{\mathrm{exp}}}{\delta D_0^{\mathrm{exp}}}\right)^{2} \tag{17}$$

where $\delta D_0^{\mathrm{exp}}$ is the error in the measured D_0 and the sum is taken over measured D_0 for target nuclei in the range $28\leq Z\leq 35$, $59\leq A\leq 83$. The resulting fit finds $\alpha=0.292885$, $\beta=-0.695180$, and $\gamma=0.034243$, and is shown in Figure 3.

At low energies, the nuclear level density is better described by a constant temperature formula:

$$\rho(E)=\frac{1}{\sqrt{2\pi}\sigma}\frac{1}{T}\exp\left[\frac{E-E_0}{T}\right] \tag{18}$$

This formula must tangentially match Equation 10 at some energy E_x that lies between Δ and the neutron binding energy. This constraint fixed E_0 and T for a given E_x, and hence E_x may be adjusted to give the best possible fit to low-lying spectroscopic levels. The spin-cutoff parameter σ is assumed to be constant below E_x. Typical values for the matching energy are $2\leq E_x\leq 8$ MeV,

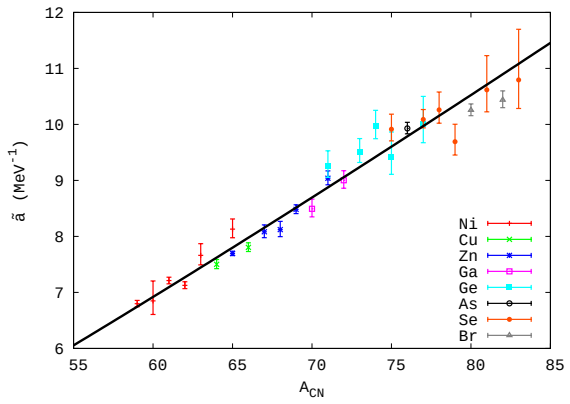

Fig. 3.— Three parameter fit to derived "experimental" asymptotic level density parameters, used to systematically determine unknown $\tilde{a}$. The data are obtained from measured s-wave resonance spacing's listed in (RIPL 1998), assuming our chosen parameterizations for the backshift and spin cutoff parameter. Our systematic, fit only to the data shown in this figure, is represented by the solid black line.

and are approximated by $E_x = 2.5 + \frac{150}{A} + \Delta$ (Gilbert & Cameron 1965).

We define the notion of achieving a "good" fit to the total level density over the entire energy range if (a) a good fit can be made to the low lying levels, (b) the observed level spacing at the neutron binding energy is exactly reproduced, and (c) the energy of the matching point E_x for the two prescriptions falls between $E = \Delta$ and $E = B_n$. Sample fits for $^{73-75}$As are shown in Figure 4.

In our attempts to match the the level density to the number of discrete levels, we generally try to ensure that the integrated level density at the energy of the last known level is equal to the cumulative number of known levels, as can be seen in each of the plots in Figure 4. This ensures that the effective level density will be continuous as the transmission coefficients shift between the discrete levels and the level density. However, there are cases where matching at the energy of the last discrete level is not possible (i.e. matching would require $E_x < \Delta$). Additional restrictions are placed on the matching energy if one requires that the nuclear temperature be positive. Occasionally the resulting lower limit on the matching energy precludes matching the last discrete level, and the integrated level density/cumulative number of levels suffers a discontinuity (recall that the Hauser-Feshbach formula only employs the level density above the energy of the last discrete level). Such

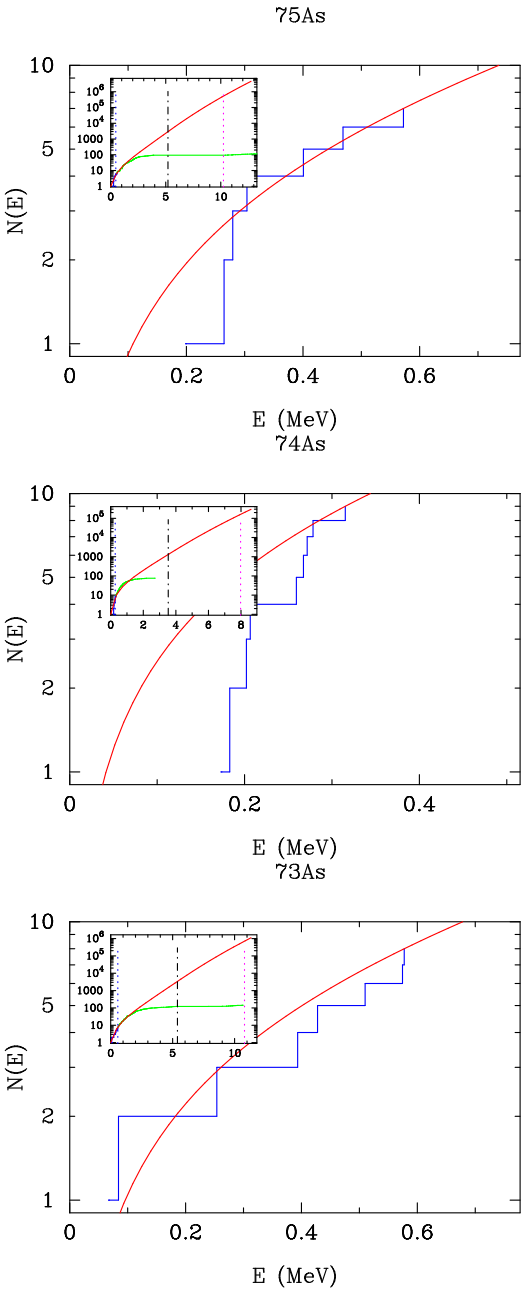

Fig. 4.— Constant temperature level density fits to the low lying spectroscopic levels of $^{73-75}$As. The known cumulative number of levels N(E) is shown in blue. The green levels, seen in the smaller insets, represent measured levels that lie above the energy at which the level scheme is considered complete. The red lines represent the integrated level density.

discontinuities have been found to result in gross non-physical behavior for some cross sections, particularly (p,n) cross sections.

In most of these cases, one can match the integrated level density to the cumulative number of levels by reducing the number of discrete levels included in the calculation. This is the approach we take. In a few instances, even a reduction in the included discrete levels could not fully rectify the situation. For those nuclei, we use the smallest allowed matching energy to reduce the size of the discontinuity as much as possible.

The fitted parameters for the total level density are presented in Table 5 (Appendix A.3). The symbols in the legend are the same as described above. In column five, an "x" indicates the level density parameter $\tilde{a}$ was derived from an experimentally known level spacing (D_0), an "s" indicates that $\tilde{a}$ was derived from the systematic shown in Figure 3.

3.4. Considerations Regarding the Exciton Pre-Equilibrium Model

We adopt a simple exciton model with initial 2-particle 1-hole configuration. Average rates for internal transitions are related by the formulas of (Williams 1970), corrected for the Pauli principle by (Cline 1972), to the absolute square of the average effective matrix element $|M|$ of the residual interactions as per Eq. (7) of (Uhl & Strohmaier 1976). The dependence of $|M|^2$ on mass number and excitation energy is

$$|M|^2 = \langle FM \rangle A^{-3} E^{-1} \tag{19}$$

The parameter $\langle FM \rangle$ may be tuned to best replicate measured cross section data. For this region, we find that a value of $\langle FM \rangle = 100$ is satisfactory. We explore the sensitivity of various cross sections to this parameter in section 4.2.1.

When including alpha particles as a possible exit channel, one should account for them in the pre-equilibrium phase of the reaction. Generally, the description of alpha particle emission in the exciton model is a straightforward extension of the description of neutron or proton emission, given the tendency of nucleons to preform alpha clusters in the nucleus. In making such an extension, one introduces a parameter ϕ which represents the probability that the incoming particle will strike a pre-formed alpha cluster (Milazzo-Colli *et al.* 1973). It follows that the larger values of ϕ will result in a higher probability of subsequent alpha emission, thus enhancing the (n,α) reactions.

In our calculations, we have chosen a value of $\phi = 0.40$, although previous considerations of alpha emission suggest that this value may fall anywhere in the range of $0.1 \leq \phi \leq 0.8$ within the mass range of interest (Milazzo-Colli *et al.* 1973). We have used our chosen value primarily because it results in (n,α) cross sections which best fit the available experimental cross section data.

Since the alpha particle emission accounts for a relatively small portion of the total reaction cross section (generally less than 20%), variations in the ϕ parameter will only have minor effects on the other cross sections.

4. Calculated Cross Sections

4.1. Comparison to Measured Cross Sections

Having developed the various input quantities based on available experimental data in the previous section, we compare cross section results of the STAPRE-H95 model to available experimentally measured cross sections on ^{75}As. Figure 5 shows our calculated activation cross section (solid black lines in all plots that follow) defined as the sum of emission (both particle emission and gamma-ray cascade) from the compound nucleus that eventually leads to the ground state of the product (final) nucleus. We also provide (where appropriate) separate cross sections that represent decay to the ground state (red lines), and any long lived isomer (blue lines, see Table 3 in Appendix A.1 for a list of the isomers and their respective half-lives). These cross sections are plotted against the available experimental data, taken from the Experimental Nuclear Reaction Data File (CSISRS 2003). Cross section data for the total, ground, and isomeric states are colored similar the modeled cross sections (grey is activation, orange is to ground, and cyan to an isomer, respectively), with different symbols distinguishing results from various experiments.

No attempt has been made to evaluate the experimental data. We provide all that is available. This provides a sense for the agreement (or uncertainty) between individual experiments and serves to illustrate the likely error associated with a given cross section. For information on a particular measurement, consult (CSISRS 2003).

Detailed discussions for each of the cross sections in Figure 5 follow.

- ^{75}As(n,γ)^{76}As: Our modeled cross section lies consistently within 30% of the measured data below 5 MeV, usually within

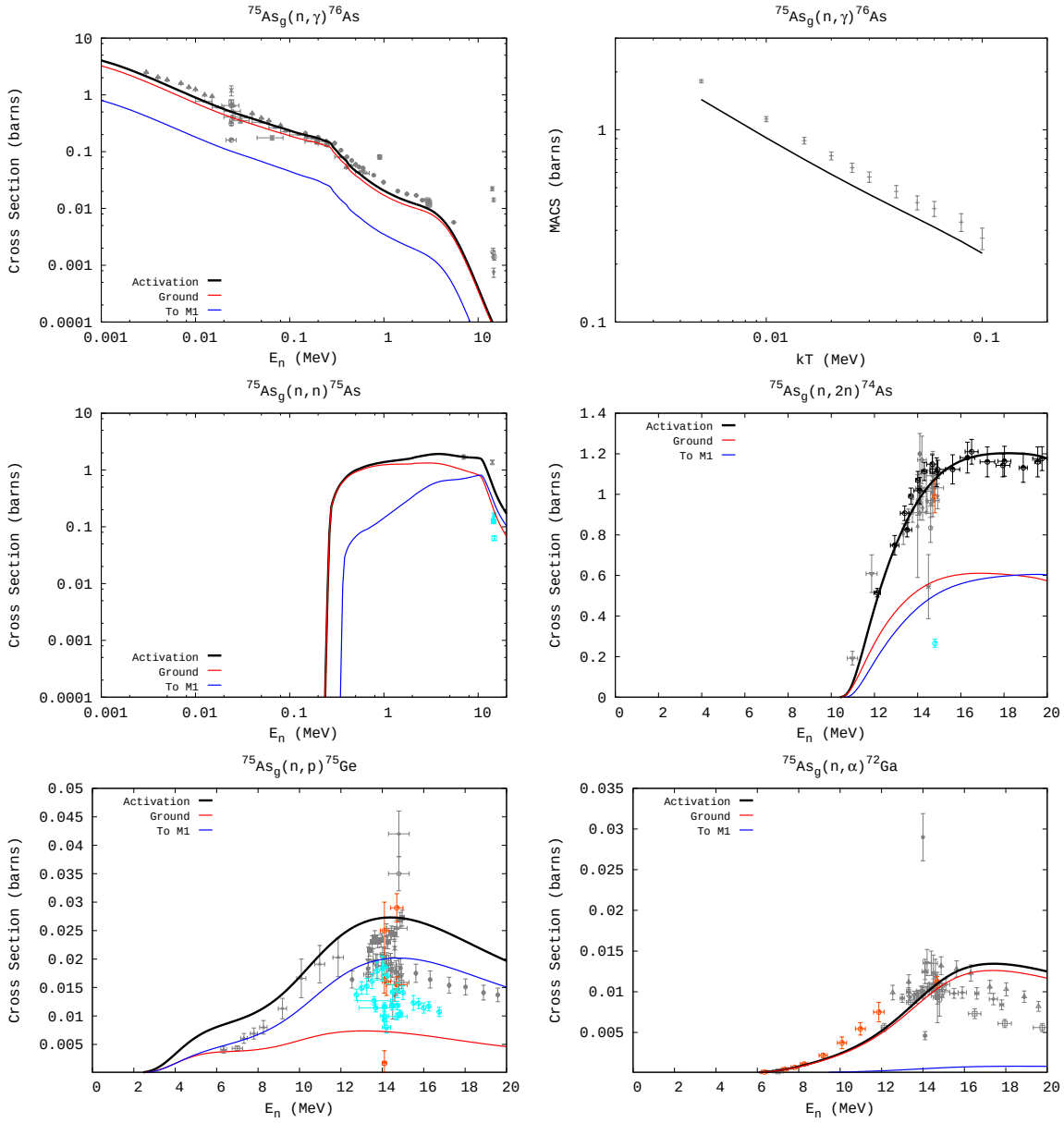

Fig. 5.— Calculated vs. measured neutron induced cross sections on ^{75}As. Measured cross sections are obtained from (CSISRS 2003). The solid black lines and grey data represent activation cross sections. Solid red lines and orange data represent the cross section going to the ground state of the residual (equal to the activation cross section when the residual nucleus does not have an isomer). Blue lines and cyan data represent the cross section going to the first isomer.

10% below 500 keV. The agreement is particularly good between 30-200 keV, where the neutron capture cross section is of greatest importance. Using global systematics, (n,γ) cross sections can typically be modeled to within a factor of two, often to within 30% (Hoffman *et al.* 1999). It should be kept in mind that for comparisons to neutron induced experimental capture cross sections we are often considering compound nuclear systems for which the important input parameters to our reaction model (e.g. those that affect level densities and photon-transmission coefficients) are determined by normalization to experimental data (e.g. from resonance analysis), and so one would

expect the comparisons to be good. Since our local systematics for these important input parameters agree well with measured data from nuclei bracketing the region of interest, we expect our other modeled capture cross sections to be of good accuracy.

We note that at roughly 14 MeV there are several measured data points. Our modeled cross section lies one or two orders of magnitude below these points. At these higher incident energies, direct reactions, which we do not include, may be playing a more significant role. We also note that at 14 MeV the value of the capture cross section is on the order of 10 millibarn or less, and is insignificant in comparison to other neutron induced reactions such as (n,2n) or (n,p) in this energy range (see Figure 5).

Yet another comparison to experimental data comes from the extensive efforts to evaluate Maxwellian averaged capture cross sections for astrophysical applications (Bao *et al.* 2000). The Maxwellian-averaged neutron capture cross section is defined as the reaction rate $\langle \sigma v \rangle$ divided by the mean velocity $v_T = \sqrt{2kT/\mu}$ at a given temperature T. Here, μ is the reduced mass. For particle fluences and temperatures typical to stellar nucleosynthesis, the velocity distribution of the neutrons reduces to a Maxwell-Boltzmann distribution. In this case, the Maxwellian-averaged cross section reduces to (Beer *et al.* 1992)

$$\frac{\langle \sigma v \rangle}{v_T} = \frac{\int_0^\infty \sigma_{n\gamma} v \Phi(v) dv}{v_T} = \frac{2}{\sqrt{\pi}(kT)^2} \int_0^\infty \sigma_{n\gamma}(E) W(E, kT) dE \quad (20)$$

where $W(E, kT) = E \exp(-E/kT)$ and E is the center of mass energy.

Using spline interpolation to determine the value of the (n,γ) cross section between points on the energy grid, and assuming a $E_{lab}^{-1/2}$ energy dependence below our lowest grid energy, our modeled (n,γ) cross section yields the Maxwellian-averaged capture cross section shown in the top-right panel of Figure 5. The experimental data is taken from a set of recommended Maxwellian-averaged capture cross sections (Bao *et al.* 2000). The error bars on all points are identical and represent the measured error for the cross section at 30 keV. Our modeled Maxwellian-averaged capture cross section has a value of 461.4 millibarns at kT = 30 keV. This value is 19% lower than that recommended by (Bao *et al.* 2000) (0.568±0.035 barns). For a comparison of recommended 30 keV Maxwellian averaged cross sections and our calculations for other nuclei with $32 \leq Z \leq 34$, see Table 1. On average, our calculations are within 32.3% of the recommended values.

Table 1: Comparison of our modeled (n,γ) Maxwellian-averaged activation cross sections to recommended values at 30 keV. Column one lists the targets for which recommended values are available. Column two lists the recommended 30 keV MACS and their uncertainties. Column three gives our calculated values for the Maxwellian-averaged neutron capture cross section at 30 keV. The last column gives the ratio of the weighted average to our calculated value. The average error shown at the bottom is the average absolute percent difference between our MACS and the recommended values.

^{A}Z	$\sigma_{rec.}$	$\sigma_{mod.}$	$\sigma_{rec.}/\sigma_{mod.}$
^{70}Ge	88 ± 5	104.780	0.840
^{72}Ge	73 ± 7	71.564	1.020
^{73}Ge	243 ± 47	354.855	0.685
^{74}Ge	53 ± 7	47.893	1.107
^{76}Ge	33 ± 15	23.493	1.405
^{75}As	568 ± 35	461.419	1.231
^{74}Se	267 ± 25	322.415	0.828
^{76}Se	164 ± 8	177.438	0.924
^{77}Se	418 ± 71	515.509	0.811
^{78}Se	109 ± 41	75.359	1.446
^{80}Se	42 ± 3	71.193	0.590
^{82}Se	9 ± 8	18.943	0.475
		Average error:	32.3%

In our comparison with measured cross section data at 30 keV (top-left panel in Figure 5) the agreement is even better. Taking a weighted average of the measured cross sections with incident energies whose errors overlap the range of 29-31 keV, with weights corresponding to the inverse geometric mean of the errors in cross section and energy (i.e. $w_i = (dE_i^2 + d\sigma_i^2)^{-1/2}$), one obtains an average 30 keV capture cross section of 452 millibarns. Our modeled cross section has

a value of 445 millibarns at 30 keV, which is lower than the average value by less than 2%.

- ^{75}As(n,n')^{75}As: Our activation cross section is in good agreement with the measured cross section at 7 MeV, but significantly lower than the measurement at 14 MeV. Again, at higher incident energies direct reactions may be playing a more significant role, and direct reactions have not been included in our calculations.

- ^{75}As(n,2n)^{74}As: Among the more important neutron induced reactions, particularly above 10 MeV, are the (n,2n) reactions. These reactions can usually be modeled with greater accuracy than neutron capture cross sections, primarily because (n,2n) cross sections have a nearly negligible dependence on photon transmission functions. As a rule of thumb (n,2n) cross sections scale roughly as the size of the nucleus and at 14 MeV a value between 0.5-2 barns. In Figure 5 we see that our modeled (n,2n) activation cross section is in excellent agreement with the available experimental data. We find that our cross section lies within 2% of the weighted mean of the measured activation cross sections at 14.7 MeV. The agreement between our calculation and the measured (n,2n) cross section populating the ground state and isomer of ^{74}As are in less satisfactory agreement. We note that the ground state and isomer measurements each consist of a single point by the same author, and sum to an activation cross section significantly larger than other activation measurements. Only two data sets span most of the energy range between threshold and 20 MeV. These data sets are highlighted (in black) on panel four of Figure 5. Our modeled cross section is in good agreement with these data sets.

  A comparison between our modeled cross section and the weighted mean of measured cross sections at 14.7±0.1 MeV for various targets with $32 \leq Z \leq 34$ is given in Table 2. The weights for the various data sets were determined by taking the inverse geometric mean of the errors in cross section and energy (i.e. $w_i = (dE_i^2 + d\sigma_i^2)^{-1/2}$). The deviation (fourth column) gives a rough indication of the amount of uncertainty between different measurements. On average, our calculations reproduce the weighted mean (n,2n) cross section at 14.7±0.1 MeV to within 13.2%.

Table 2: Comparison of our modeled (n,2n) activation cross sections to measured values at 14.7±0.1 MeV. Column one lists the targets for which measured data is available. Column two lists the number of data points that fall in the bin of 14.7±0.1 MeV. Column three is a weighted average of the data in the bin, in barns, as described in the text. Column four gives the standard deviation of the data points from the weighted average, in barns. Column five lists our calculated values for the (n,2n) cross section at 14.7 MeV. The last column gives the ratio of the weighted average to our calculated value. The average error shown at the bottom is the average absolute percent difference between our cross sections and the weighted averages.

^{A}Z	N	$\bar{\sigma}$	Dev.	$\sigma_{mod.}$	$\bar{\sigma}/\sigma_{mod.}$
^{70}Ge	15	0.670	0.256	0.663	1.011
^{76}Ge	9	1.200	0.112	1.365	0.879
^{75}As	10	1.058	0.059	1.064	0.994
^{74}Se	2	0.604	0.254	0.445	1.356
^{76}Se	8	0.932	0.147	1.002	0.930
^{78}Se	1	0.951	0.000	1.123	0.847
^{80}Se	1	1.043	0.000	1.332	0.783
^{82}Se	3	1.265	0.160	1.403	0.902
				Average error:	13.2%

- ^{75}As(n,p)^{75}Ge: Our modeled cross section tends to be higher than the measurements by roughly 50% depending on which data set one compares to. At 14.7 MeV, our cross section is larger than the weighted mean of the data by ∼25%. We have found similar difficulties replicating (n,p) cross sections in other regions (Hoffman *et al.* 2004a; Hoffman *et al.* 2004b; Hoffman *et al.* 2004c; Kelley *et al.* 2005). However, we note that the (n,p) cross section is quite small in comparison to (n,2n). Additionally, in producing the activities of interest, namely ^{73,74}As, the (n,p) reactions will be of minor import, since production of these activities involving (n,p) would necessarily involve a subsequent proton induced reaction.

- ^{75}As(n,α)^{72}Ga: Our modeled cross section is in reasonable agreement with experiment up to ∼15 MeV. Keep in mind that the parameters related to alpha particle emission

in the exciton model employed in our calculations can be tuned to reproduce (n,α) cross sections without significantly changing other cross sections. Again, since the (n,α) cross sections are small and can only be involved in the production of ^{73,74}As through less probable secondary reactions, their effect will be of little import.

Overall, we find our modeling effort satisfactory relative to reproducing measured cross sections on ^{75}As.

4.2. Sensitivity Studies

We now illustrate the sensitivity of our modeled results to variations in the input parameters developed in §3 against the measured activation cross sections for (n,γ) and (n,2n) on ^{75}As.

4.2.1. Sensitivity to the Pre-Equilibrium Cross Section

Figure 6 shows the sensitivity of the ^{75}As(n,2n) cross section to variations of $50 \leq \langle FM \rangle \leq 400$ (§3.4). The neutron capture cross section on the same target will not exhibit any sensitivity to this parameter since pre-equilibrium is unimportant at the low energies where neutron capture cross sections are large. The overall effect of varying $\langle FM \rangle$ is that larger values of $\langle FM \rangle$ result in larger (n,2n) cross sections. An opposite effect appears in the (n,p) cross sections (not shown), with larger values of $\langle FM \rangle$ tending to result in smaller cross sections at higher energies. We find that a value of $\langle FM \rangle = 100$ provides the best agreement with the ^{75}As(n,2n)^{74}As cross section. This same value was applied in calculating the pre-equilibrium contribution to all cross sections in this study.

4.2.2. Sensitivity to the choice of Level Density Prescription

The nuclear level density parameters developed for this study (§3.3, Appendix 5) reflect best choices from the available experimental data in the region of interest. Instead of varying each of the many parameters ($a(U,Z,N), \sigma^2, \lambda, \Delta, \delta_W$), we instead present results where only the overall treatment of the level density prescription was varied, keeping all other parameter input fixed.

Figure 7 shows the experimental cross sections for (n,γ) and (n,2n) cross sections on ^{75}As. Only data for the activation cross section is shown. For comparison we show our local systematic level density (red-solid line, Appendix 5).

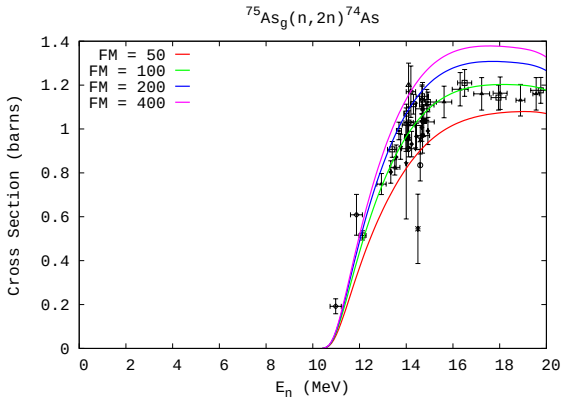

Fig. 6.— Sensitivity of ^{75}As(n,2n)^{74}As cross section to the pre-equilibrium matrix element. The black data points are activation cross section data (CSISRS 2003). The red, green, blue, and magenta lines correspond to our calculated activation cross section using $\langle FM \rangle$ of 50, 100, 200, and 400, respectively.

The second level density prescription (Rauscher *et al.* 1997) is plotted as the green solid line. This prescription is the current standard used in the calculation of cross sections for use in stellar nucleosynthesis calculations (Rauscher *et al.* 2002). This prescription is similar to ours, in that it also embodies an energy dependent $a(E)$ parameter (e.g. (Iljinov *et al.* 1992)) with shell corrections that damp out with increasing excitation energy. It differs from ours in the parameterization of the asymptotic value of the $\tilde{a}$ parameter (Section 3.3, Figure 3).

The third level density prescription (Gilbert & Cameron 1965) is plotted as a solid blue line. These level densities do not include an energy dependent $\tilde{a}$, and also differ in the parameterization of the backshift and spin cutoff parameter.

The last choice (magenta-solid line) reflects a recent attempt to calculate level densities using microscopic nuclear structure models (Goriely 2002).

For the (n,γ) capture reactions, we see that all three level density prescriptions result in a similar cross section below 5 MeV, although the overall scale is lower for the (Rauscher *et al.* 1997) level densities. This is due primarily to the fact that the larger level densities will result in a larger calculated s-wave radiation width, and therefore require a smaller overall normalization to the gamma ray

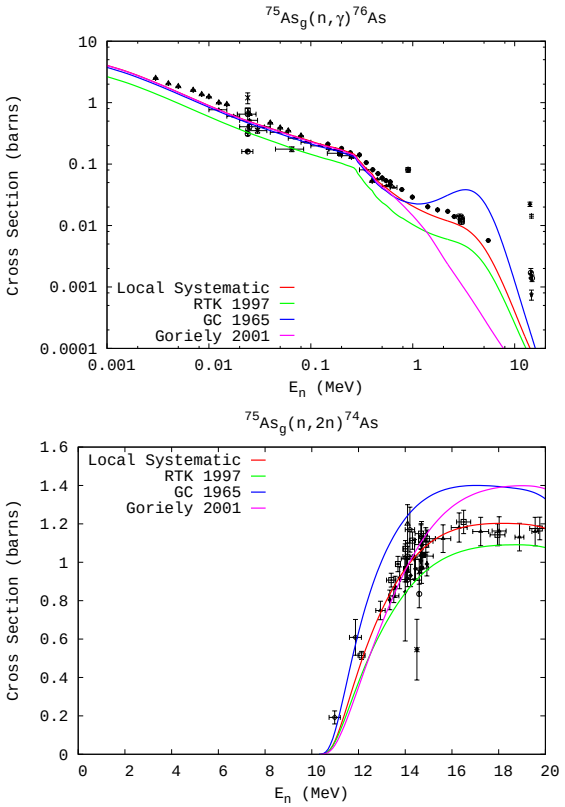

Fig. 7.— Sensitivity of ^{75}As(n,γ) and ^{75}As(n,2n) cross sections to the level density prescription. The black data corresponds to measured activation cross sections taken from (CSISRS 2003). The red solid line represents our calculation using our local level density systematic. The green and blue lines represent calculations using the level density prescriptions of (Rauscher *et al.* 1997) and (Gilbert & Cameron 1965), respectively. The magenta lines represent calculations using the level densities of (Goriely 2002).

strength function. For this reason, we see that the shape of the cross section is the same at energies below 500 keV (since the Hauser-Feshbach formula is using the discrete level data as opposed to the level density), but the size of the cross section varies. The other three level density prescriptions do a reasonably good job in modeling the neutron capture cross section at low energies, but have markedly different behaviors above ∼1 MeV. We find that our local level density prescription is preferable to the other three in replicating this cross section.

For the (n,2n) reaction we see that the four level density prescriptions produce significantly different cross sections. Again, we find that our local

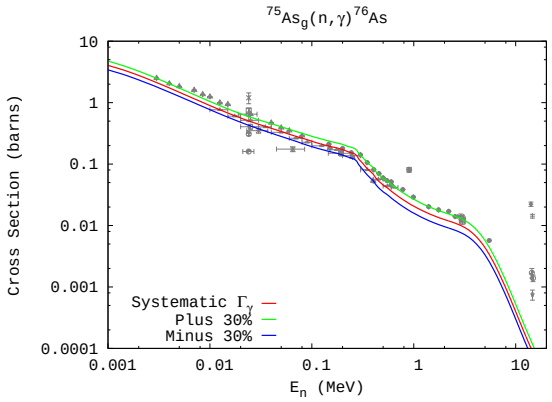

Fig. 8.— Sensitivity to a ±30% adjustment of the experimental *s*-wave average photon width. The black data represents measured activation cross sections taken from (CSISRS 2003). The red line represents our calculation, and the green and blue lines represent our calculation with a ±30% adjustment to the *s*-wave radiation width. The total difference in the cross section is ∼17-30%.

systematic to be preferable to any of the other three.

4.2.3. Sensitivity to the Normalization of the γ-ray Transmission Coefficient

The γ-ray transmission coefficient (§3.2.3) is significantly smaller than the particle transmission coefficients that enter into the statistical model. Consequently, for neutron capture reactions, one finds that the cross section is roughly proportional to T_γ, multiplied by a relevant energy dependence. Hence, one would expect that any adjustment to the normalization of the γ-ray transmission coefficient would have a corresponding effect on the capture cross sections. For instance, if the normalization constant is increased by a factor of two, the cross section should also increase by approximately a factor of two.

Figure 8 shows the sensitivity to a ±30% change to the value of the average *s*-wave photon width used to normalize the gamma-ray transmission coefficients. This translates into a roughly 17% change in the cross section below 30 keV, rising to ∼25-30% at 1 MeV and above. The (n,2n) cross section will not exhibit any sensitivity to T_γ because it is much smaller than the particle transmission functions and only enters into Eq. [1] in the denominator. In general, the smaller of the two transmission coefficients in the HF numerator will be the one that determines the cross section, especially if one is much smaller. This is always

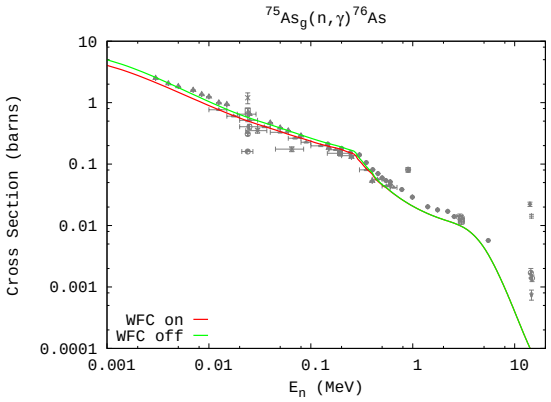

Fig. 9.— Sensitivity to inclusion or exclusion of width fluctuation corrections. The black data represents measured activation cross sections taken from (CSISRS 2003). The red line represents our calculation, and the green line represents our calculation excluding WFC.

the case with photon vs. particle widths.

The mean error associated with the experimental values of the gamma ray strength function for isotopes ranging from nickel to bromine is 23.0% with a standard deviation of 9.3%. Hence, the uncertainties related to the gamma ray strength function in the capture cross sections will be generally smaller than that shown in Figure 8.

4.2.4. Sensitivity to the Inclusion of Width Fluctuation Corrections

We adopt the Moldauer model of the Width Fluctuation Corrections (§2.3) as embodied in the STAPRE code. For targets in the mass range of interest which have available experimental data, reaction thresholds are always greater than several MeV, and inclusion/exclusion of width fluctuation corrections will only be evident for capture reactions. Figure 9 shows the affect for the activation capture cross sections of ^{75}As, both with (solid red line) and without (solid green line) WFC. As expected a decrease in the capture cross section is noticeable, and is as large as 20% at 1 keV and roughly 14% at 30 keV. When the projectile energy increases, the capture cross section declines rapidly and the elastic enhancement vanishes, disappearing almost completely by 1 MeV. The (n,p) channel does not open until the incident neutron energy is above 2 MeV, and thus no other channels can compete with the elastic and capture cross sections before the WFC are negligible.

4.3. Production and Destruction Cross Sections

Figure 10 shows the modeled cross sections that directly affect the production and destruction of ^{73}As and ^{74}As. Identical plots for the other targets that span a slightly wider N range of the original detector sets are presented in Appendix B.

Since we are considering only neutron induced reactions, the capture and (n,2n) cross sections are the only significant production channels for both isotopes. The (n,3n) channel is the only other production channel considered, and the thresholds for both of these reactions are above 15 MeV.

For the destruction reactions, (n,γ) dominates below ∼1 MeV, although ^{74}As(n,p)^{74}Ge does not have a threshold and competes at lower incident energies. The (n,p) reaction is dominant between ∼1-10 MeV in both cases. ^{73}As(n,np+pn)^{72}Ge becomes significant between 7-10 MeV. Above 10 MeV, (n,2n) is the dominant destruction channel. In all cases, the (n,α) and (n,d) channels are comparatively small. Refer to Appendix B for the cross sections of greatest importance in the production and destruction of other arsenic isotopes.

5. Conclusions

We have developed a new neutron threshold cross section set for radiochemical diagnostics of ^{73,74}As. The theory and implementation of the Hauser-Feshbach model were described (§2), along with the details of the local systematics used to create a set of input parameters that reflect the latest available experimental data in the region of interest (§3). Sensitivity of the modeled cross sections to the input models and their parameters has been explored (§4). The choice of our developed local systematics appears to do reasonably well in replicating measured cross sections on ^{75}As (Figure 5).

The (n,2n) cross sections displayed large sensitivity to the prescription for the nuclear level densities and the choice of the pre-equilibrium matrix element FM. Our locally developed nuclear level density parameterization proved superior to three other popular choices for a variety of reaction channels (Figure 7). Coupled with this, our choice for FM provided consistently good agreement with experimental data over the entire region of interest (Figure 6). For (n,γ) capture reactions the largest sensitivity remains the normalization of the photon transmission functions (§3.2.3, Figure 8). Our systematics to predict these quanti-

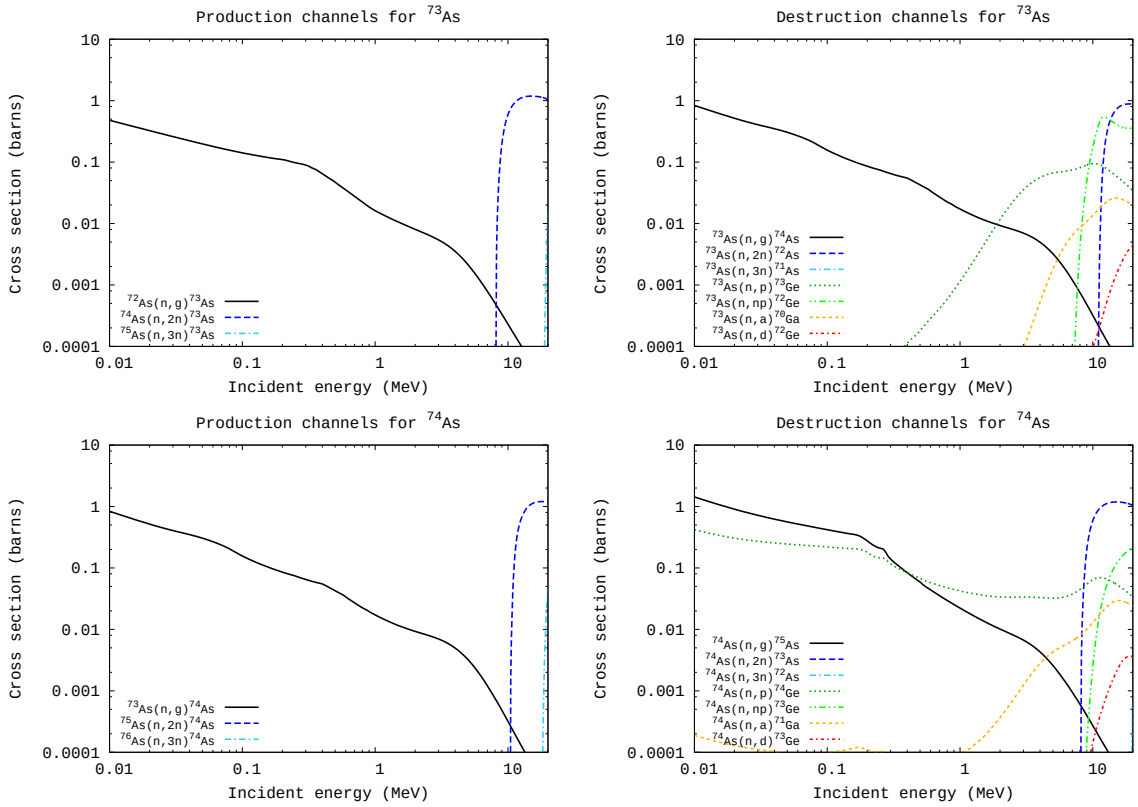

Fig. 10.— Calculated cross sections directly affecting production and destruction of ^{73,74}As.

ties when experimental data is not available are of similar quality as those developed for previous detector sets.

Overall we consider the modeling effort to be quite successful, as our calculated cross sections do agree favorably with experimentally measured ones in this region of interest. Our calculations agree on average with measured (n,2n) cross sections to roughly 13% (often better, see Table 2), which is representative of the spread in the existing experimental cross sections. Our neutron capture cross sections agree to roughly 30% (Table 1). We identified these as the largest cross sections that can produce and destroy ^{73,74}As respectively, although we note that (n,p) reactions on these two isotopes could dominate destruction for incident neutron energies between roughly 1 and 5 MeV (Figure 10).

6. Acknowledgments

This work was performed under the auspices of the U.S. Department of Energy by the University of California Lawrence Livermore National Laboratory under contract W-7405-ENG-48.

REFERENCES

Avrigeanu, M. & Avrigeanu, V. IPNE-Bucharest Report No. NP-86-1995 (September 1995) http://www.nea.fr/abs/html/iaea0971.html

Bao, Z. Y., Beer, H., Kappeler, F.,, Voss, F., & Wisshak, K., 2000, Atomic Data & Nuclear Data Tables, **76**, 70

Beer, H., Voss, F., & Winters, R. R., 1992, ApJS, **80**, 403

Experimental Nuclear Reaction Data File, Brookhaven National Laboratory, US Dept. of Energy, http://www.nndc.bnl.gov/nndc/exfor/

Cline, C. K., 1972, Nucl. Phys. **A195**, 353

ENSDF: Evaluated Nuclear Structure Data File, Brookhaven National Laboratory, US Dept. of Energy, http://www.nndc.bnl.gov/nndc/ensdf/

Gilbert, A., & Cameron, A.G.W., 1965, Can. J. Phys., **43**, 1446

Demetriou, P., & Goriely, S., 2001, Nucl. Phys. **A695**, 95

Hauser, W., & Feshbach, H., 1952, Phys. Rev. **87**, 366

Hilaire, S., Lagrange, Ch., & Koning, A. J., 2003, Ann. of Phys. **306**, 209

Hofmann, H.M., Richert, J, Tepel, J. W. & Weidenmu̇ller, H.A., 1975, Ann. of Phys. **90**, 403

Hoffman, R. D., Rauscher, T., Woosley, S. E. & Thielemann, F.-K., 1999, ApJ, **521**, 735

Hoffman, R.D., Dietrich, F.S., Bauer, R., Kelley, K., and Mustafa, M., 2004, UCRL-TR-205563 (Br-Kr)

Hoffman, R.D., Dietrich, F.S., Bauer, R., Kelley, K., and Mustafa, M., 2004, UCRL-TR-206721 (I-Xe)

Hoffman, R.D., Dietrich, F.S., Bauer, R., Kelley, K., and Mustafa, M., 2004, UCRL-TR-211558 (Sm-Eu-Gd)

Kelley, K., Hoffman, R.D., Dietrich, F.S., Bauer, R., and Mustafa, M., 2005, UCRL-TR-211668 (Ti-V, Cr-Mn, Fe)

Iljinov, A.S., Mebel, M.V., Bianchi, N., De Sanctis, E., Guaraldo, C., Lucherini, V., Muccifora, V., Polli, E., Reolon, A.R., & Rossi, P. 1992, Nucl. Phys. **A543**, 517

Koning, A.J., & Delaroche, J.P., 2003, Nucl. Phys. **A713**, 231

McFadden, L., and Satchler, G.R., 1966, Nuc. Phys. **84**, 177

Milazzo-Colli, L., and Braga-Marcazzan, G.M., 1973, Nuc. Phys. **A210**, 297

Moldauer, P. A., 1976, Phys. Rev. **C14** 764

Möller, P., Nix, J.R., Myers, W.D., & Swiatecki, W.J., 1995, Atomic Data & Nuclear Data Tables, **59**, 185

Nethaway, D.R., Memo, "The Cross-Section Sets Used With the Watusi Program." LLNL A-Division memo, 5 Nov., 1998

Perey, C.M. and Perey, F.G., 1963, Phys. Rev. **132**, 755

Pruet, J., 2005, UCRL-TR-210452

Rauscher, T., Thielemann, F.-K., & Kratz, K.-L. 1997, Phys. Rev. C., **56**, 1613

Rauscher, T., Heger, A. Hoffman, R. D. & Woosley, S. E., 2002, ApJ, **576**, 323

Raynal, J. "ECIS96", Proceedings of the Specialists' Meeting on the Nucleon Nucleus Optical Model up to 200 MeV, 13-15 November 1996, Bruyeres-le-Chatel, Franc (http://www.nea.fr/html/science/om200/raynal.pdf)

Handbook for calculations of nuclear reaction data, Reference input parameter library. 1998, IAEA-TECDOC-1034

Uhl, M., & Strohmaier, B. IRK-Vienna Report IRK-76/01 1976 (Upd. 1978)

Vonach, H., 1982, UCID-19549, LLNL

Wapstra, A.H., Audi, G., & Thibault, C., 2003, Nuc. Phys. **A729**, 129

Williams, F. C. Jr., 1970, Phys. Lett. **31B**, 184

This 2-column preprint was prepared with the AAS LaTeX macros v5.0.

A. Basic Nuclear Structure Data

A.1. Adopted Spins, Parities, Binding Energies, and Separation Energies

Table 3:: Spins, parities, binding energies, and separation energies

^{A}Z	J^{π}	BE (MeV)	S_n (MeV)	S_p(MeV)	S_α (MeV)	S_d (MeV)
^{68}Ni	0+	590.408	7.793	15.692	11.118	20.488
^{64}Cu	1+	559.301	7.916	7.201	6.200	11.814
^{65}Cu	3/2-	569.211	9.911	7.453	6.790	14.887
^{66}Cu	1+	576.277	7.066	8.421	7.252	12.295
^{67}Cu	3/2-	585.409	9.132	8.601	7.903	15.328
^{68}Cu	1+	591.729	6.320	9.113	8.199	12.696
^{69}Cu	3/2-	599.969	8.240	9.561	8.991	15.129
^{70}Cu	1+	605.280	5.311	10.287	9.290	12.648
^{71}Cu	3/2-	613.087	7.806	10.850	10.075	15.868
^{66}Zn	0+	578.136	11.059	8.925	4.578	16.611
^{67}Zn	5/2-	585.188	7.052	8.911	4.793	13.753
^{68}Zn	0+	595.386	10.198	9.977	5.333	16.885
^{69}Zn	1/2-	601.869	6.482	10.140	5.717	14.235
^{70}Zn	0+	611.086	9.218	11.117	5.983	17.133
^{71}Zn	1/2-	616.920	5.834	11.640	6.009	14.726
^{72}Zn	0+	625.796	8.876	12.709	7.092	18.291
^{73}Zn	1/2-	631.146	5.350	12.916	7.857	15.835
^{65}Ga	3/2-	563.040	11.894	3.942	3.098	13.580
^{66}Ga	0+	572.179	9.139	5.102	3.352	10.856
^{67}Ga	3/2-	583.405	11.227	5.269	3.725	14.104
^{68}Ga	1+	591.683	8.278	6.495	4.087	11.322
^{69}Ga	3/2-	601.996	10.313	6.609	4.489	14.583
^{70}Ga	1+	609.649	7.654	7.781	5.077	12.038
^{71}Ga	3/2-	618.951	9.302	7.865	5.246	14.858
^{72}Ga	3-	625.471	6.520	8.552	5.447	12.160
^{73}Ga	3/2-	634.653	9.181	8.857	6.388	15.508
^{74}Ga	3-	641.074	6.422	9.928	7.498	13.054
^{75}Ga	3/2-	649.561	8.486	10.045	8.178	16.190
^{76}Ga	2+	655.464	5.903	11.117	8.939	13.723
^{67}Ge	1/2-	578.401	9.105	6.222	2.870	13.136
^{68}Ge	0+	590.794	12.393	7.389	3.401	16.391
^{69}Ge	5/2-	598.986	8.192	7.303	3.614	13.357
^{70}Ge	0+	610.520	11.534	8.524	4.089	16.613
^{71}Ge	1/2-	617.936	7.416	8.287	4.452	13.716
^{72}Ge	0+	628.686	10.750	9.735	5.004	16.812
^{73}Ge	9/2+	635.469	6.783	9.997	5.304	14.293
^{74}Ge	0+	645.665	10.196	11.012	6.283	17.969
^{75}Ge	1/2-	652.170	6.505	11.096	6.954	15.293
^{76}Ge	0+	661.598	9.428	12.037	7.507	18.299
^{77}Ge	7/2+	667.670	6.072	12.206	8.229	15.885
^{68}As	3+	581.931	10.323	3.530	2.490	10.410
^{69}As	5/2-	594.190	12.259	3.396	2.854	13.565
^{70}As	0+	603.518	9.328	4.532	3.044	10.499
^{71}As	5/2-	615.140	11.622	4.620	3.440	13.929
^{72}As	2-	623.547	8.407	5.611	3.569	10.802
^{73}As	3/2-	634.345	10.798	5.660	4.054	14.185
^{73}As$_{m1}$	9/2+	(-0.428)	(-0.428)	(-0.428)	(-0.428)	(-0.428)

Table 3: (continued)

^{A}Z	J^{π}	BE (MeV)	S_n (MeV)	S_p(MeV)	S_α (MeV)	S_d (MeV)
^{74}As	2-	642.320	7.975	6.851	4.375	11.410
^{74}As$_{m1}$	4+	(-0.259)	(-0.259)	(-0.259)	(-0.259)	(-0.259)
^{75}As	3/2-	652.564	10.244	6.899	5.317	14.871
^{75}As$_{m1}$	9/2+	(-0.304)	(-0.304)	(-0.304)	(-0.304)	(-0.304)
^{76}As	2-	659.892	7.328	7.722	6.125	12.003
^{76}As$_{m1}$	1+	(-0.044)	(-0.044)	(-0.044)	(-0.044)	(-0.044)
^{77}As	3/2-	669.591	9.698	7.993	6.642	15.196
^{77}As$_{m1}$	9/2+	(-0.475)	(-0.475)	(-0.475)	(-0.475)	(-0.475)
^{78}As	2-	676.563	6.972	8.892	7.193	12.740
^{72}Se	0+	622.429	12.849	7.289	3.340	16.687
^{73}Se	9/2+	630.824	8.394	7.277	3.542	13.459
^{74}Se	0+	642.890	12.066	8.545	4.075	17.119
^{75}Se	5/2+	650.918	8.028	8.598	4.686	14.348
^{76}Se	0+	662.072	11.154	9.509	5.091	17.528
^{77}Se	1/2-	669.491	7.419	9.599	5.727	14.703
^{78}Se	0+	679.989	10.498	10.398	6.029	17.872
^{75}Br	3/2-	647.106	11.904	4.215	3.670	14.057
^{76}Br	1-	656.327	9.221	5.409	4.484	11.212
^{77}Br	3/2-	667.344	11.017	5.272	4.703	14.202
^{78}Br	1+	675.633	8.289	6.142	5.017	11.336
^{79}Br	3/2-	686.320	10.688	6.331	5.461	14.605

A.2. Q-values for Select Reactions

Table 4:: Q-values for activation reactions studied, in MeV

^{A}Z	(n,g)	(n,2n)	(n,3n)	(n,p)	(n,np)	(n,a)	(n,d)
^{71}As	8.407	-11.622	-20.950	2.796	-4.620	4.838	-2.396
^{72}As	10.798	-8.407	-20.029	5.139	-5.611	6.744	-3.386
^{73}As	7.975	-10.798	-19.205	1.123	-5.660	3.600	-3.435
^{74}As	10.244	-7.975	-18.773	3.345	-6.851	4.927	-4.627
^{75}As	7.328	-10.244	-18.218	-0.394	-6.899	1.203	-4.674
^{76}As	9.698	-7.328	-17.572	1.706	-7.722	3.056	-5.497
^{77}As	6.972	-9.698	-17.027	-1.920	-7.992	-0.221	-5.768

A.3. Nuclear Level Density Parameters

Table 5:: Adopted level density parameters

^{A}Z	$\tilde{a}(A)$ (MeV)$^{-1}$	Δ (MeV)	δW (MeV)	x/s	$\sigma^2(E_x)$	E_x (MeV)	E_0 (MeV)	T (MeV)	N
^{68}Ni	8.335	2.334	1.020	s	3.476	6.711	-0.790	0.947	2
^{64}Cu	7.501	-0.643	2.420	x	3.424	4.092	-4.063	1.019	16
^{65}Cu	7.799	0.343	2.330	s	2.095	1.000	-0.954	0.774	14
^{66}Cu	7.804	-0.639	2.690	x	3.497	4.237	-4.170	0.998	6
^{67}Cu	8.155	0.359	2.360	s	2.111	1.000	-0.864	0.733	0
^{68}Cu	8.335	-0.737	2.620	s	2.197	0.000	-1.840	0.680	3
^{69}Cu	8.514	0.343	2.300	s	2.155	1.000	-0.789	0.689	0
^{70}Cu	8.694	-0.962	2.510	s	3.159	2.000	-3.114	0.788	0
^{71}Cu	8.875	0.201	1.910	s	3.570	4.814	-3.118	0.912	0
^{66}Zn	7.977	1.916	2.890	s	3.405	6.422	-1.348	0.954	10
^{67}Zn	8.083	-0.182	3.160	x	3.405	4.194	-3.355	0.932	8
^{68}Zn	8.121	1.771	2.990	x	3.592	6.925	-1.979	0.988	31
^{69}Zn	8.483	-0.094	3.330	x	3.016	2.489	-1.999	0.758	4
^{70}Zn	8.694	1.659	2.940	s	3.599	6.701	-2.010	0.939	2
^{71}Zn	9.038	0.011	3.250	x	3.536	4.713	-3.410	0.888	2
^{72}Zn	9.056	1.844	2.590	s	3.542	6.289	-1.368	0.878	3
^{73}Zn	9.238	-0.008	2.430	s	3.592	4.547	-3.300	0.877	1
^{65}Ga	7.799	0.110	2.980	s	3.349	4.460	-3.040	0.955	6
^{66}Ga	7.977	-0.802	3.400	s	3.692	5.500	-5.452	1.072	37
^{67}Ga	8.155	0.207	3.690	s	3.191	3.672	-2.313	0.847	6
^{68}Ga	8.335	-0.711	3.890	s	3.439	3.854	-4.041	0.916	23
^{69}Ga	8.514	0.186	3.790	s	3.100	3.119	-1.957	0.778	5
^{70}Ga	8.493	-0.538	3.940	x	3.483	3.913	-3.784	0.896	26
^{71}Ga	8.875	0.228	3.710	s	3.514	4.793	-3.101	0.882	3
^{72}Ga	9.003	-1.027	3.920	x	3.777	4.890	-5.415	0.962	12
^{73}Ga	9.238	0.151	3.370	s	3.170	3.000	-1.919	0.734	0
^{74}Ga	9.420	-0.808	2.860	s	3.598	3.719	-4.091	0.858	0
^{75}Ga	9.603	0.148	2.090	s	3.525	4.126	-2.712	0.819	6
^{76}Ga	9.786	-0.738	1.710	s	3.503	3.000	-3.416	0.797	0
^{67}Ge	8.155	-0.149	3.740	s	3.215	3.426	-2.749	0.855	4
^{68}Ge	8.335	2.049	3.670	s	3.426	6.515	-1.202	0.912	6
^{69}Ge	8.514	-0.142	4.190	s	3.405	4.165	-3.285	0.880	20
^{70}Ge	8.694	2.005	4.130	s	3.427	6.299	-1.126	0.868	14
^{71}Ge	9.261	-0.164	4.300	x	3.271	3.480	-2.814	0.783	8
^{72}Ge	9.056	2.010	4.080	s	3.596	6.932	-1.602	0.891	4
^{73}Ge	9.511	-0.067	4.190	x	3.690	5.420	-4.134	0.899	8
^{74}Ge	9.966	1.951	3.820	x	3.632	7.059	-1.812	0.854	6
^{75}Ge	9.419	0.113	3.750	x	3.890	6.161	-4.384	0.946	9
^{76}Ge	9.786	1.850	2.530	s	3.655	6.387	-1.435	0.842	6
^{77}Ge	10.012	0.167	2.150	x	3.733	4.948	-3.295	0.852	4
^{68}As	8.335	-0.774	3.830	s	3.656	5.031	-5.058	1.004	4
^{69}As	8.514	0.020	3.760	s	3.139	3.100	-2.225	0.791	9
^{70}As	8.694	-0.956	4.320	s	3.400	3.227	-4.008	0.857	30
^{71}As	8.875	0.137	4.350	s	3.465	4.531	-3.076	0.861	9
^{72}As	9.056	-1.014	4.480	s	3.593	3.946	-4.669	0.888	47
^{73}As	9.238	-0.015	4.370	s	3.698	5.386	-4.016	0.908	8
^{74}As	9.420	-1.004	4.410	s	3.561	3.533	-4.331	0.838	9
^{75}As	9.603	0.076	4.080	s	3.704	5.205	-3.705	0.872	7

Table 5: (continued)

^{A}Z	$\tilde{a}(A)$ $(\mathrm{MeV})^{-1}$	Δ (MeV)	δW (MeV)	x/s	$\sigma^2(E_x)$	E_x (MeV)	E_0 (MeV)	T (MeV)	N
^{76}As	9.928	-1.062	4.030	x	3.714	4.056	-4.839	0.854	22
^{77}As	9.970	0.080	3.020	s	3.594	4.279	-2.963	0.802	12
^{78}As	10.154	-0.854	2.620	s	2.954	1.000	-2.248	0.615	0
^{72}Se	9.056	2.180	4.330	s	3.526	6.763	-1.178	0.864	1
^{73}Se	9.238	-0.193	4.670	s	3.535	4.362	-3.539	0.846	1
^{74}Se	9.420	2.092	4.420	s	3.694	7.343	-1.794	0.886	8
^{75}Se	9.914	0.016	4.480	x	3.702	5.351	-3.948	0.863	26
^{76}Se	9.786	1.993	4.080	s	3.776	7.391	-2.004	0.879	17
^{77}Se	10.088	0.095	4.060	x	3.707	5.044	-3.553	0.834	17
^{78}Se	10.260	1.900	3.270	x	3.755	6.864	-1.737	0.836	17
^{75}Br	9.603	-0.066	4.650	s	3.701	5.121	-3.912	0.869	19
^{76}Br	9.786	-0.889	4.610	s	3.644	3.866	-4.395	0.830	24
^{77}Br	9.970	-0.058	4.280	s	3.779	5.249	-3.994	0.861	25
^{78}Br	10.154	-1.134	4.210	s	3.739	3.822	-4.792	0.829	24
^{79}Br	10.339	0.003	4.070	s	3.713	4.691	-3.442	0.804	26

A.4. Adopted Level Schemes for $^{72-76}$As

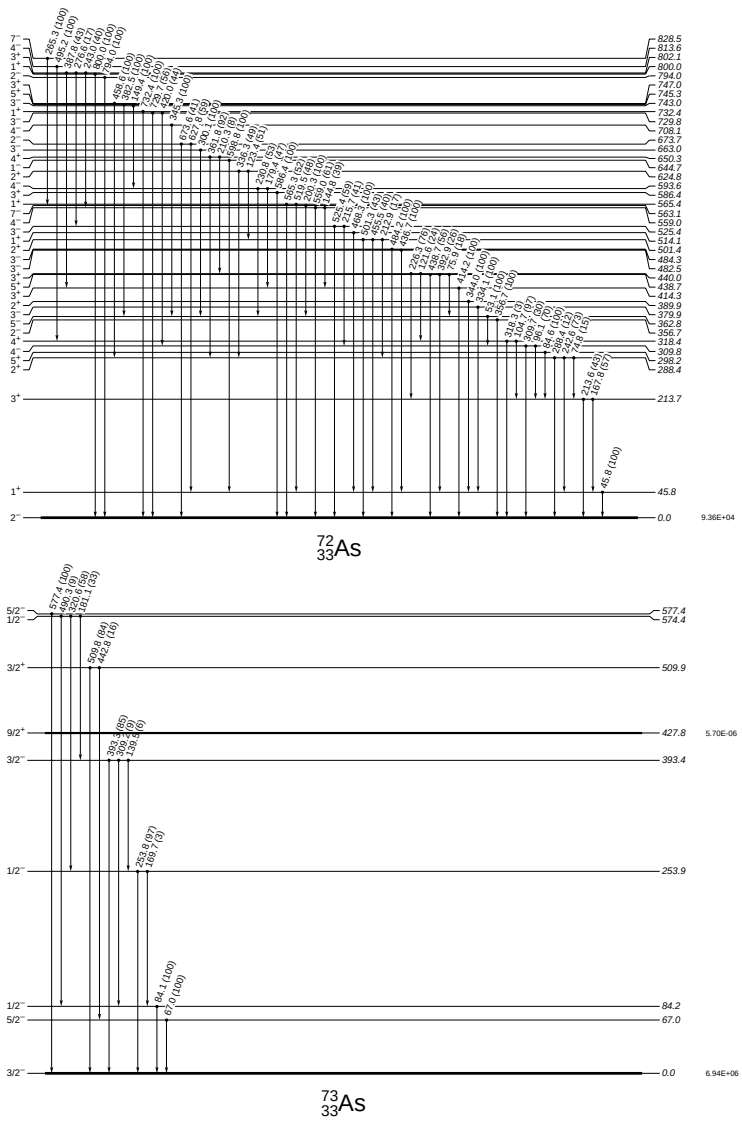

Fig. 11.— Adopted level schemes for $^{72-76}$As

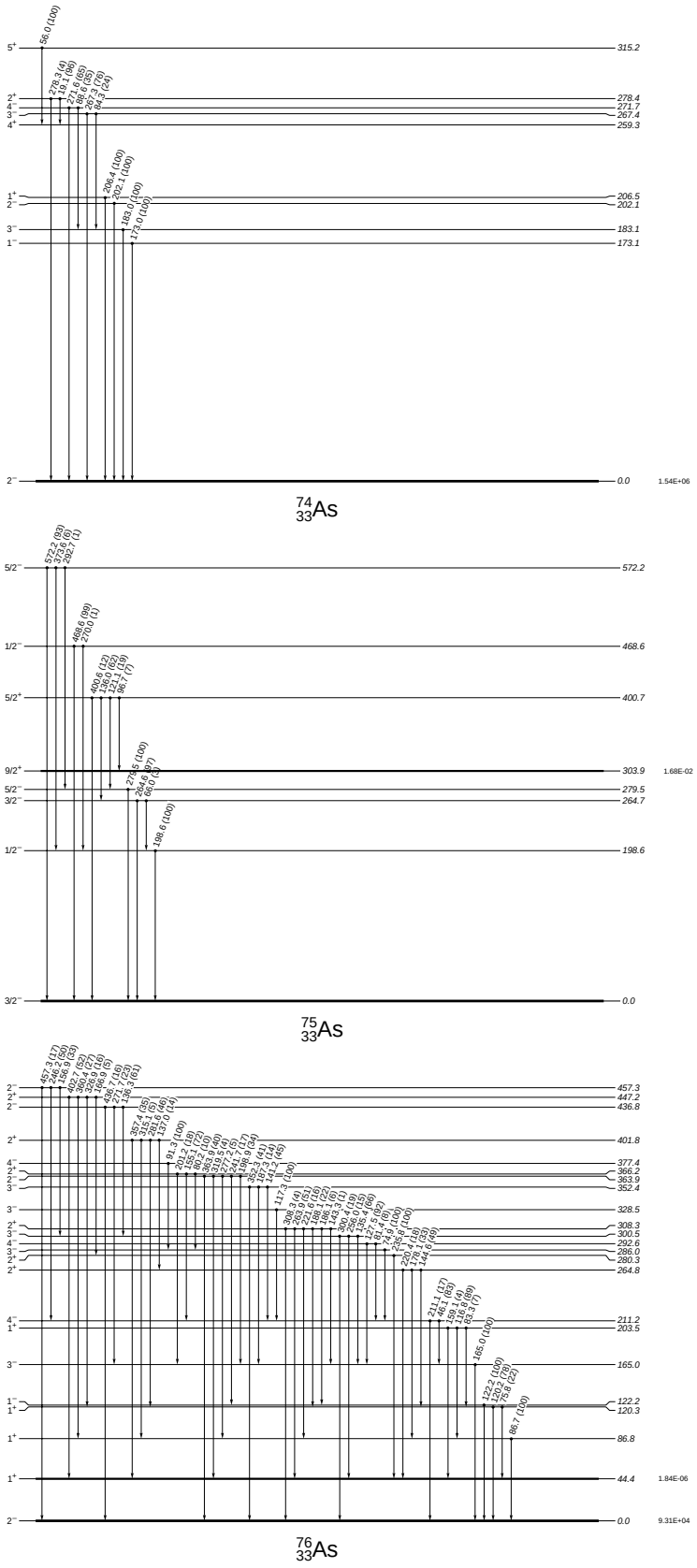

Fig. 11.— (continued)

B. Modeled Cross Sections: Production and Destruction Channels

Here we present the activation cross sections for the various neutron induced reaction channels producing a given isotope and destroying the ground state of that isotope.

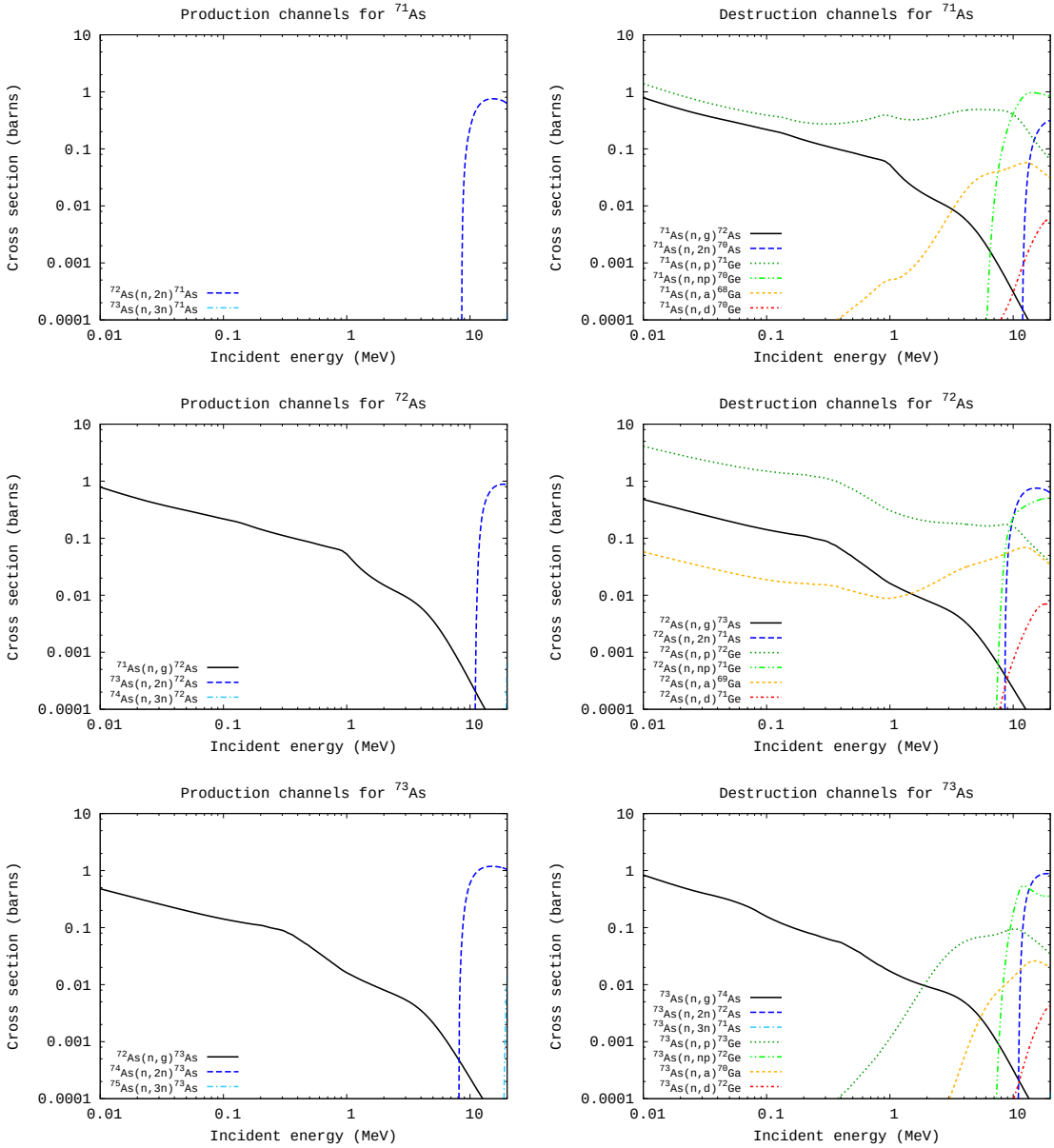

Fig. 12.— Production and destruction cross sections

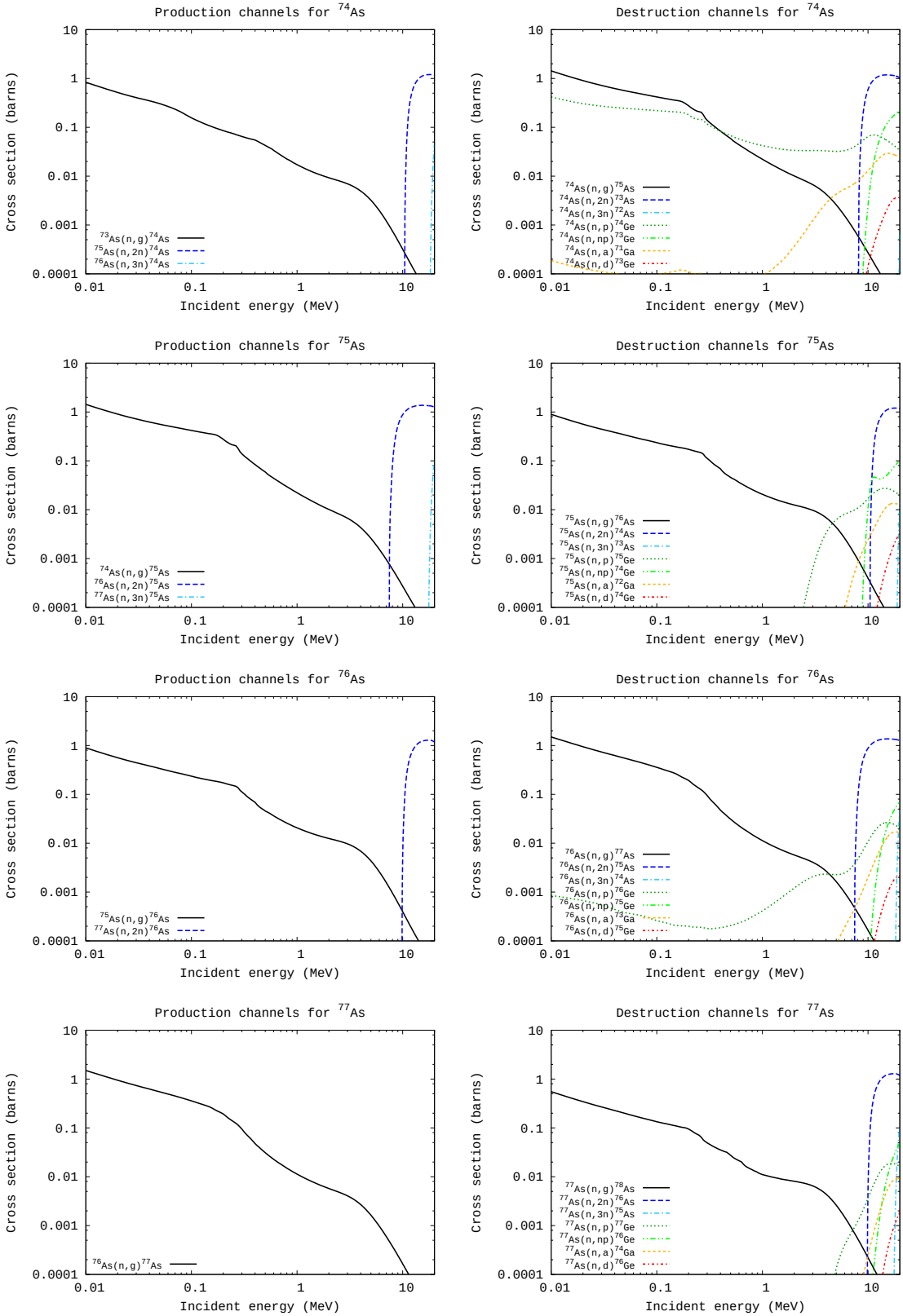

Fig. 12.— (continued)